AIAA OK

NASA Technical Memorandum 82894

Aerodynamic Performance of High Turning Core Turbine Vanes in a Two-Dimensional Cascade

John R. Schwab
Lewis Research Center
Cleveland, Ohio

Prepared for the
Eighteenth Joint Propulsion Conference
cosponsored by the AIAA, SAE, and ASME
Cleveland, Ohio, June 21-23, 1982

NASA

AERODYNAMIC PERFORMANCE OF HIGH TURNING CORE TURBINE VANES IN A TWO-DIMENSIONAL CASCADE

John R. Schwab
National Aeronautics and Space Administration
Lewis Research Center
Cleveland, Ohio

Summary

Experimental and theoretical aerodynamic performance data are presented for four uncooled high turning core turbine vanes with exit angles of 74.9, 75.0, 77.5, and 79.6 degrees in a two-dimensional cascade. Data for a more conservative 67.0 degree vane are included for comparison. Correction of the experimental aftermix kinetic energy losses to a common 0.100 centimeter trailing edge thickness yields a linear trend of increased loss from 0.020 to 0.025 as the vane exit angle increases from 67.0 to 79.6 degrees. The theoretical losses show a similar trend. The experimental and theoretical vane surface velocity distributions generally agree within approximately five percent, although the suction surface theoretical velocities are generally higher than the experimental velocities as the vane exit angle increases.

Introduction

The increased specific work requirements for the core turbines in advanced high bypass ratio turbofan engines are forcing the stator vane exit angle to approach 90 degrees from the axial direction in order to maintain an acceptable vane height. Aerodynamic performance data for such high turning vanes are not readily available, since most present core turbines have exit angles of less than 70 degrees.

A research program has been underway at the NASA Lewis Research Center to investigate the performance of high turning vanes. This paper presents experimental and theoretical kinetic energy loss coefficients and surface velocity distributions for four uncooled vane designs with exit angles of 74.9, 75.0, 77.5, and 79.6 degrees. A more conservative 67.0 degree vane was also tested to provide data for comparison.

The experimental data were obtained by testing constant-section solid vanes in a two-dimensional cascade with inlet room temperature air. Cross-channel surveys of total pressure, static pressure, and flow angle were conducted for ideal exit critical velocity ratios of 0.65 to 0.95. The loss coefficients were calculated from the actual and ideal velocities. Vane surface static pressures were also measured and used to calculate the vane surface airflow velocities.

The theoretical data were obtained from a finite difference inviscid stream function solution on the vane-to-vane stream surface (refs. 1

and 2). The theoretical vane surface velocity distributions were used as input to an integral method boundary layer solution (ref. 3), which provided boundary layer parameters for an aerodynamic loss calculation (ref. 4) to obtain the loss coefficients.

Symbols

b	trailing edge blockage factor, $t/s \cos \alpha$
c_x	vane axial chord, cm
$\bar{e}$	kinetic energy loss coefficient, $1 - (V/V_{id})^2$
p	absolute pressure, N/cm^2
s	vane pitch, cm
t	trailing edge thickness, cm
V	velocity, m/sec
w	mass flow rate per unit vane span, kg/sec-cm
α	flow angle, degrees
δ	ratio of inlet total pressure to U.S. standard sea-level atmospheric pressure, $p_0'/10.132\ N/cm^2$
θ_{cr}	ratio of inlet critical velocity to critical velocity of U.S. standard sea-level air, $V_{cr,0}/310.6$ m/sec
σ_x	axial solidity factor, c_x/s
Ψ	Zweifel loading factor

Subscripts:

cr	critical condition
id	ideal process
s	vane surface
0	vane inlet station
1	vane exit station
2	aftermix station

Superscript:

' total state condition

Apparatus and Procedure

Vane Design

The design parameters for the subject vanes are given in table 1. Velocity diagrams for all the vanes except the 67.0° vane were selected with a meanline turbine design calculation using the data given in table 2. These conditions are representative of an advanced high bypass ratio turbofan engine. For a fixed stator exit angle, the mean diameter was varied parametrically to obtain a subsonic stator and rotor while maintaining a suitable blade height (hub-to-tip diameter ratio of less than 0.85). The design stator exit velocity ratio was selected such that the absolute stator exit velocity was equal to the relative rotor exit velocity. This criterion minimized the stage kinetic energy in order to minimize losses. Since the 74.9° and 79.6° vanes were originally designed using different criteria, the optimum diameters and exit velocities determined for the new conditions were different from those in the original design. Through judicious selection of the number of vanes for the new diameters, the vane pitch, axial solidity, and Zweifel loading were maintained very close to the original design values. Since the 67.0° vane was used as a standard to compare the performance of the high turning vanes against, the original design velocity diagram was used. The vane profiles and coordinates are shown in figure 1, while the four high turning vanes are shown in the photograph in figure 2.

Cascade Tunnel

The vanes were tested in the two-dimensional cascade tunnel shown in figure 3. The test sections consisted of 7, 8, or 9 constant-section solid vanes, depending on the vane pitch, with a span of 10.2 centimeters.

In operation, room air was drawn through the cascade tunnel, the test section, and the exhaust control valves into the laboratory exhaust system. The vanes were tested over a range of inlet total pressure to exit static pressure ratios corresponding to ideal exit critical velocity ratios from 0.65 to 0.95.

Instrumentation

The center vane in each test section was instrumented at midspan with static pressure taps. The vane surface static pressures were measured with a multichannel scanner using a strain gage transducer. The pressure data were recorded by the laboratory data acquisition system.

The vane exit total pressure, static pressure, and flow angle were surveyed simultaneously using the rake shown in figure 4. The total pressure was measured with a square-ended probe while the static pressure was measured with a wedge probe having an included angle of 15 degrees. The

angle probe was a two-tube type with the tube ends cut at 45 degrees; it measured a differential pressure proportional to the flow angle. The probes were calibrated over a range of velocities and angles in an open-jet tunnel.

The rake was fixed at the design aftermix flow angle which placed the probe sensing elements at the survey plane shown in figure 5. The rake was traversed over a distance of approximately two vane pitches in order to obtain a full wake profile. The traverse speed was 2.5 centimeters per minute. An actuator-driven potentiometer provided a voltage signal proportional to the rake position. This signal and the output of the three strain gage transducers used to measure the probe pressures were recorded by the laboratory data acquisition system. Typical total and static pressure data for an aftermix survey are shown in figure 6.

Data Reduction

Vane surface critical velocity ratios were calculated from the recorded surface static pressure data. The recorded flow angle and pressure data from the surveys were used to calculate velocity, mass flow, and tangential and axial components of momentum as a function of the probe position. These quantities were then integrated to obtain the overall values at the survey plane. The aftermix kinetic energy loss coefficient, $\bar{e}_2$, was calculated at the hypothetical aftermix station where flow conditions were assumed to be uniform downstream of the survey plane by assuming a constant area process and conservation of the tangential component of momentum. The details of these calculations can be found in Appendix B of reference 5.

Theoretical Analysis

A finite difference inviscid stream function solution on the vane-to-vane stream surface (refs. 1 and 2) was used to obtain the theoretical vane surface velocity distributions. The stream sheet thickness values used in the code were modified to account for the effects of boundary layer growth and contraction on the endwalls of the cascade tunnel and the test section. A one percent total pressure loss from vane inlet to exit was assumed. The theoretical surface velocity distributions were then used as input for an integral method boundary layer code (ref. 3). This code provided boundary layer parameters for an aerodynamic loss calculation (ref.4). Transition from laminar to turbulent was forced to occur where laminar instability was predicted by the code, which corresponded to a momentum thickness Reynolds number of 200-300.

Results and Discussion

Overall Performance

The experimental aftermix kinetic energy loss coefficients, $\bar{e}_2$, are shown in figure 7 along with the theoretical loss for each vane at the design ideal aftermix critical velocity ratio. The repeatability of the experimental data is approximately ±0.0025. The experimental and theoretical losses agree within ±0.005.

The experimental and theoretical aftermix flow angle data are shown in figure 8. The uncertainty in the experimental data is primarily dependent

upon the accuracy of the probe reference angle which is approximately ±0.5 degrees. The experimental and theoretical angles agree within the limits of this uncertainty, although the experimental angles are slightly larger than the theoretical angles.

The experimental and theoretical total equivalent mass flow data are shown in figure 9. These data are presented as mass flow per unit of vane height. The experimental and theoretical data agree within approximately ± 0.001 kg/sec-cm.

Surface Velocity Distributions

The experimental and theoretical surface velocity distributions are shown in figure 10. The data show excellent agreement on the pressure surface for all the vanes; however, the agreement on the suction surface is generally not as good, especially for the vanes with larger exit angles.

The 67.0° vane has excellent agreement over the first 80 percent axial chord on the suction surface, but then the theoretical data begin to show diffusion eariler than the experimental data. The 74.9°, 75.0°, and 77.5° vanes all have good agreement within approximately 5 percent on the suction surface; the agreement for the 74.9° and 75.0° vanes is better than that for the 77.5° vane. The theoretical data for the 79.6° vane have a peak about 10 percent higher than the experimental data from 40 to 70 percent axial chord on the suction surface. It appears that the solution becomes unstable in such a region of high curvature. The agreement over the last 30 percent axial chord is excellent. The suction surface velocities for all the vanes were generally higher than the experimental velocities as the vane exit angle increased.

Kinetic Energy Loss Coefficients

In order to eliminate the incomparabilty caused by different trailing edge thicknesses, the experimental loss data were corrected to a common 0.100 centimeter trailing edge thickness using the one percent loss per ten percent blockage relationship suggested in reference 6. This thickness is representative of that required for cooling purposes in an advanced high bypass ratio turbofan engine. The theoretical losses were also recalculated using the common thickness. These data are presented in figure 11 at the design ideal aftermix critical velocity ratio for each vane. A linear trend in the experimental data of increased loss from 0.020 to 0.025 can be seen as the vane exit angle increases from 67.0 to 79.6 degrees. Although the theoretical data appear to exhibit a nonlinear trend, they are in close agreement with the experimental data, with the exception of the 79.6° vane, which has a theoretical loss 0.005 higher than the experimental loss.

Since the theoretical surface velocity distributions used to calculate the theoretical losses had higher peak velocities than the experimental distributions, the boundary layer and loss calculations were redone using the experimental distributions. These data are presented in figure 12 at the design ideal aftermix critical velocity ratio for each vane. The two vanes with the largest exit angles, 77.5 and 79.6 degrees, had the largest deviation in the theoretical distributions and subsequently show a 0.0025

reduction in predicted loss and better agreement with the experimental loss data when the experimental distribution is used.

Summary of Results

Four uncooled high turning vane designs with exit angles of 74.9, 75.0, 77.5, and 79.6 degrees were tested in a two-dimensional cascade to obtain experimental aerodynamic performance data. Theoretical performance data were obtained from an inviscid vane-to-vane stream surface code and a boundary layer code. A more conservative 67.0 degree vane was also tested to provide data for comparison.

When the experimental aftermix kinetic energy loss data were corrected to a common 0.100 centimeter trailing edge thickness, a linear trend of increased loss from 0.020 to 0.025 was shown as the vane exit angle increased from 67.0 to 79.6 degrees. The theoretical losses calculated for the common thickness showed a similar trend, but with somewhat higher losses for the 77.5° and 79.6° vanes. Subsequent recalculation of the theoretical losses using the experimental surface velocity distributions showed a 0.0025 reduction in predicted losses for the 77.5° and 79.6° vanes and thus better agreement with the experimental loss data.

The theoretical surface velocities obtained from the inviscid solution agreed with the experimental distributions within approximately five percent for all the vanes except the 79.6° vane, which had an unsubstantiated peak in the theoretical distribution. The theoretical suction surface velocities were generally higher than the experimental velocities as the vane exit angle increased.

References

1. Katsanis, Theodore: FORTRAN Program for Calculating Transonic Velocities on a Blade-to-Blade Stream Surface of a Turbomachine. NASA TN D-5427, 1969.

2. Wood, Jerry R.: Improved Method for Calculating Transonic Velocities on Blade-to-Blade Stream Surfaces of a Turbomachine. NASA TP-1772, 1981.

3. McNally, William D.: FORTRAN Program for Calculating Compressible Laminar and Turbulent Boundary Layers in Arbitrary Pressure Gradients. NASA TN D-5681, 1970.

4. Stewart, Warner L.: Analysis of Two-Dimensional Compressible Flow Loss Characteristics Downstream of Turbomachine Blade Rows in terms of Boundary Layer Characteristics. NASA TN-3515, 1955.

5. Goldman, Louis J.; and McLallin, Kerry L.: Cold-Air Annular-Cascade Investigation of Aerodynamic Performance of Cooled Turbine Vanes. I - Facility Description and Base (Solid) Vane Performance. NASA TM X-3006, 1974.

6. Prust, Herman W.; Moffitt, Thomas P.; and Bider, Bernard: Effect of Varible Stator Area on Performance of a Single-Stage Turbine Suitable for Air Cooling. V - Stator Detailed Losses with 70-Percent Design Area. NASA TM X-1696, 1968.

TABLE 1 - VANE DESIGN PARAMETERS

Aftermix flow angle, α, degrees	Aftermix velocity ratio, $(V/V_{cr})_2$	Trailing-edge blockage factor, b	Axial solidity factor, σ_x	Zweifel loading factor, Ψ
67.0	0.778	0.111	0.929	0.774
74.9	.843	.079	.716	.701
75.0	.833	.122	.630	.792
77.5	.810	.124	.537	.790
79.6	.795	.076	.439	.813

TABLE 2 - TURBINE DESIGN PARAMETERS

Inlet total temperature, T_0', K.	1533
Inlet total pressures, p_0', N/cm^2.	124.1
Mass flow, w, kg/sec.	27.21
Rotative speed, N, rpm.	13000
Specific work output, $\Delta h'$, J/g.	288.7
Total efficiency, η, percent.	0.89
Overall stator pressure loss, $(p_0' - p_2')/p_0'$, percent	0.02

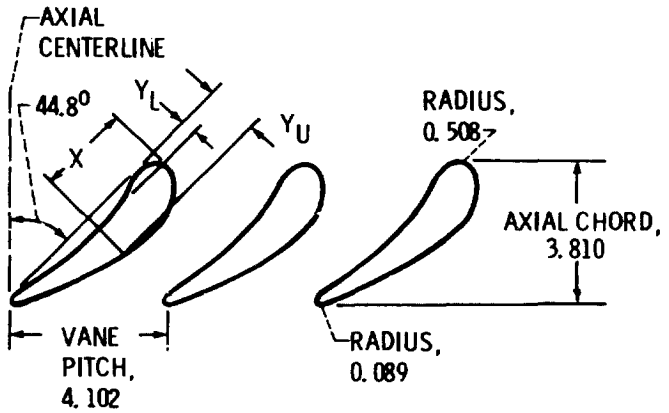

X	Y_L	Y_U	X	Y_L	Y_U
0.000	0.509	0.509	3.000	0.379	1.204
0.200	0.105	0.935	3.200	0.368	1.143
0.400	0.012	1.128	3.400	0.352	1.078
0.600	0.008	1.266	3.600	0.332	1.008
0.800	0.080	1.361	3.800	0.308	0.935
1.000	0.158	1.423	4.000	0.280	0.858
1.200	0.223	1.460	4.200	0.248	0.777
1.400	0.274	1.477	4.400	0.213	0.691
1.600	0.314	1.477	4.600	0.176	0.603
1.800	0.343	1.462	4.800	0.136	0.511
2.000	0.364	1.437	5.000	0.095	0.415
2.200	0.378	1.402	5.200	0.053	0.316
2.400	0.386	1.361	5.400	0.009	0.214
2.600	0.389	1.313	5.539	0.088	0.088
2.800	0.386	1.261			

(a) For 67.0° vane.

Figure 1. - Geometry (dimensions in cm).

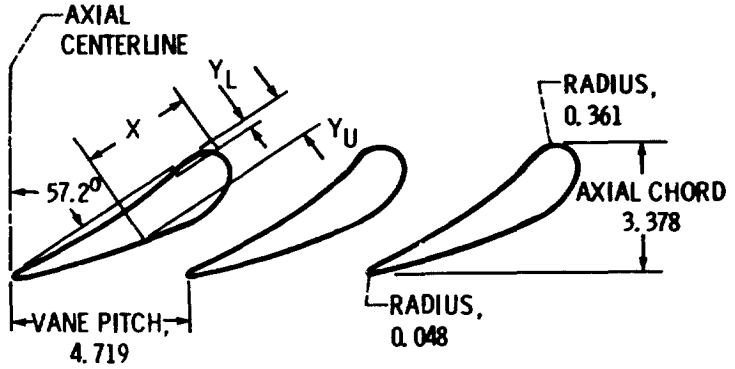

X	Y_L	Y_U	X	Y_L	Y_U
0.000	0.361	0.361	3.400	0.294	1.031
0.200	0.038	1.152	3.600	0.292	0.975
0.400	0.002	1.276	3.800	0.287	0.918
0.600	0.043	1.353	4.000	0.278	0.859
0.800	0.083	1.399	4.200	0.267	0.799
1.000	0.118	1.422	4.400	0.254	0.739
1.200	0.149	1.430	4.600	0.237	0.677
1.400	0.178	1.425	4.800	0.218	0.614
1.600	0.204	1.410	5.000	0.197	0.550
1.800	0.225	1.387	5.200	0.174	0.485
2.000	0.243	1.357	5.400	0.148	0.419
2.200	0.257	1.321	5.600	0.120	0.352
2.400	0.269	1.281	5.800	0.089	0.284
2.600	0.278	1.236	6.000	0.057	0.215
2.800	0.286	1.188	6.200	0.022	0.145
3.000	0.291	1.138	6.377	0.048	0.048
3.200	0.294	1.086			

(b) For 74.9° vane.

Figure 1. - Continued.

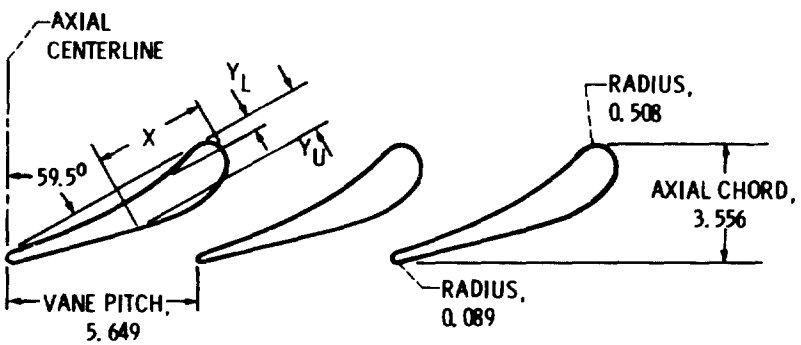

X	Y_L	Y_U	X	Y_L	Y_U
0.000	0.509	0.509	3.800	0.587	1.133
0.200	0.105	1.064	4.000	0.568	1.084
0.400	0.012	1.221	4.200	0.546	1.035
0.600	0.008	1.319	4.400	0.520	0.983
0.800	0.089	1.385	4.600	0.492	0.930
1.000	0.193	1.427	4.800	0.460	0.875
1.200	0.283	1.453	5.000	0.425	0.819
1.400	0.361	1.465	5.200	0.388	0.762
1.600	0.427	1.468	5.400	0.349	0.703
1.800	0.481	1.461	5.600	0.308	0.643
2.000	0.525	1.447	5.800	0.264	0.582
2.200	0.559	1.427	6.000	0.219	0.520
2.400	0.585	1.402	6.200	0.173	0.457
2.600	0.603	1.372	6.400	0.127	0.394
2.800	0.614	1.339	6.600	0.083	0.329
3.000	0.619	1.303	6.800	0.042	0.263
3.200	0.619	1.264	7.000	0.006	0.197
3.400	0.613	1.224	7.134	0.088	0.088
3.600	0.602	1.179			

(c) For 75.0° vane.

Figure 1. - Continued.

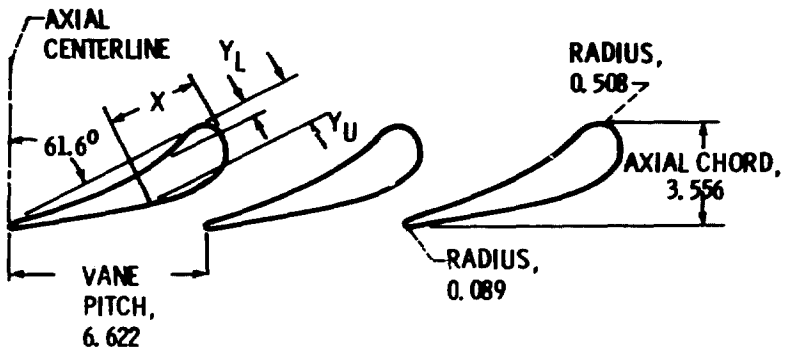

X	Y_L	Y_U	X	Y_L	Y_U
0.000	0.508	0.508	4.000	0.439	1.310
0.200	0.104	1.411	4.200	0.425	1.255
0.400	0.012	1.580	4.400	0.409	1.198
0.600	0.008	1.676	4.600	0.391	1.140
0.800	0.091	1.733	4.800	0.371	1.080
1.000	0.191	1.765	5.000	0.351	1.019
1.200	0.266	1.779	5.200	0.328	0.957
1.400	0.323	1.781	5.400	0.305	0.893
1.600	0.368	1.771	5.600	0.280	0.829
1.800	0.402	1.755	5.800	0.254	0.764
2.000	0.428	1.732	6.000	0.228	0.699
2.200	0.448	1.704	6.200	0.200	0.632
2.400	0.462	1.672	6.400	0.171	0.564
2.600	0.471	1.636	6.600	0.142	0.496
2.800	0.475	1.597	6.800	0.111	0.428
3.000	0.477	1.555	7.000	0.080	0.359
3.200	0.474	1.510	7.200	0.048	0.289
3.400	0.469	1.463	7.400	0.016	0.219
3.600	0.462	1.414	7.591	0.089	0.089
3.800	0.452	1.363			

(d) For 77.5° vane.

Figure 1. - Continued.

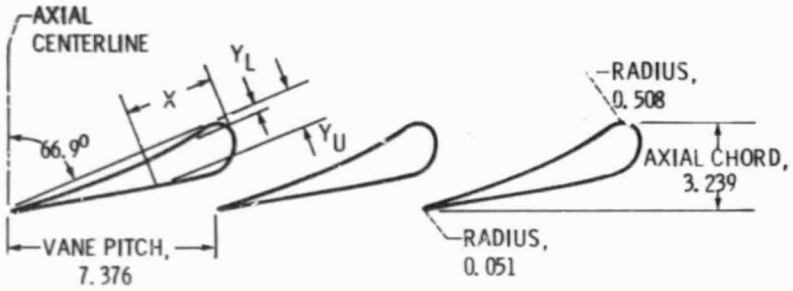

X	Y_L	Y_U	X	Y_L	Y_U
0.000	0.509	0.509	4.400	0.345	1.101
0.200	0.104	1.459	4.600	0.341	1.054
0.400	0.012	1.568	4.800	0.335	1.006
0.600	0.008	1.629	5.000	0.328	0.958
0.800	0.066	1.661	5.200	0.320	0.910
1.000	0.117	1.674	5.400	0.311	0.862
1.200	0.160	1.673	5.600	0.300	0.813
1.400	0.196	1.662	5.800	0.289	0.764
1.600	0.227	1.644	6.000	0.276	0.714
1.800	0.252	1.620	6.200	0.262	0.665
2.000	0.272	1.592	6.400	0.248	0.615
2.200	0.290	1.560	6.600	0.232	0.565
2.400	0.304	1.526	6.800	0.215	0.514
2.600	0.315	1.489	7.000	0.196	0.464
2.800	0.325	1.450	7.200	0.176	0.413
3.000	0.333	1.410	7.400	0.153	0.363
3.200	0.339	1.369	7.600	0.128	0.312
3.400	0.344	1.326	7.800	0.101	0.261
3.600	0.347	1.283	8.000	0.070	0.209
3.800	0.349	1.238	8.200	0.037	0.158
4.000	0.349	1.193	8.400	0.001	0.107
4.200	0.348	1.147	8.463	0.051	0.051

(e) For 79.6^0 vane.

Figure 1. - Concluded.

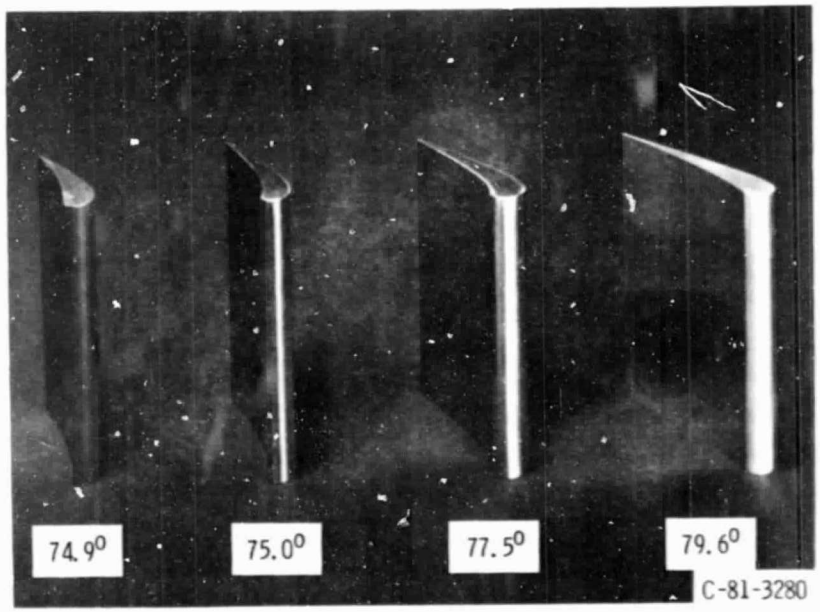

Figure 2. - Two-dimensional constant section vanes.

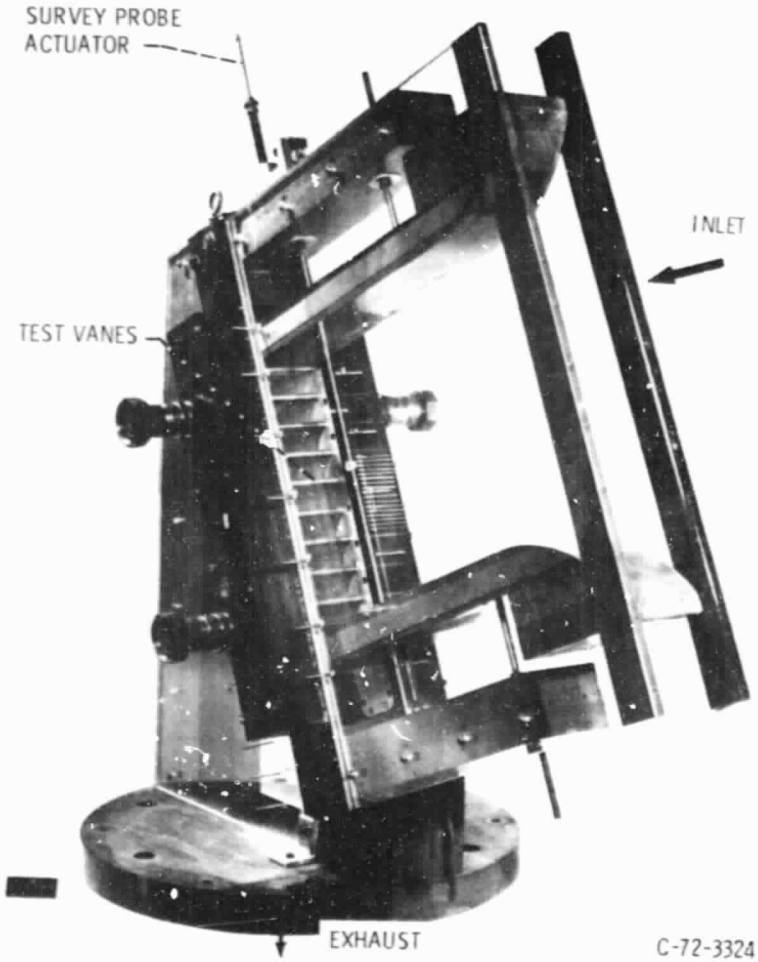

Figure 3. - Cascade tunnel.

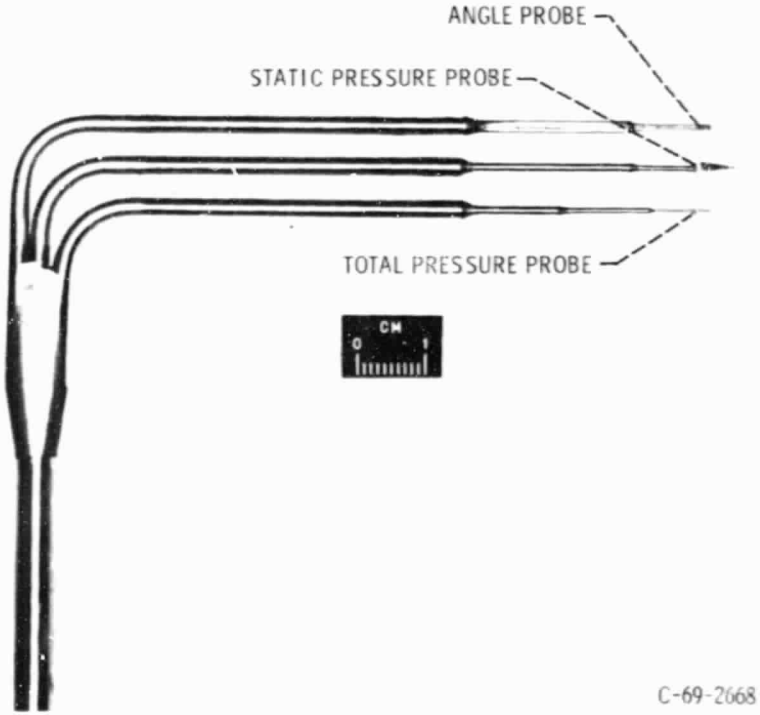

Figure 4. - Vane exit survey rake.

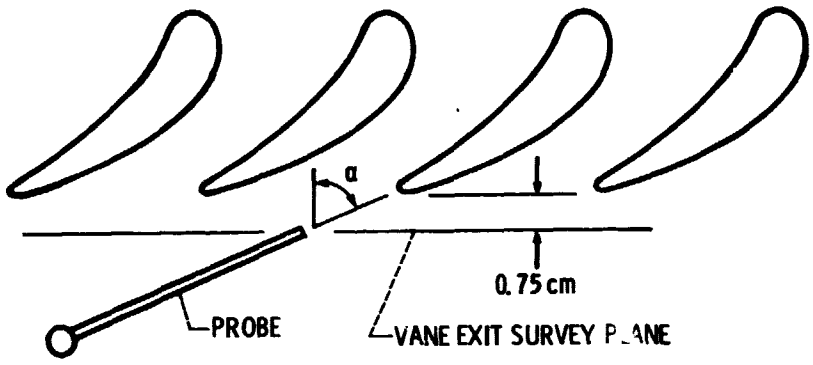

Figure 5. - Survey plane geometry.

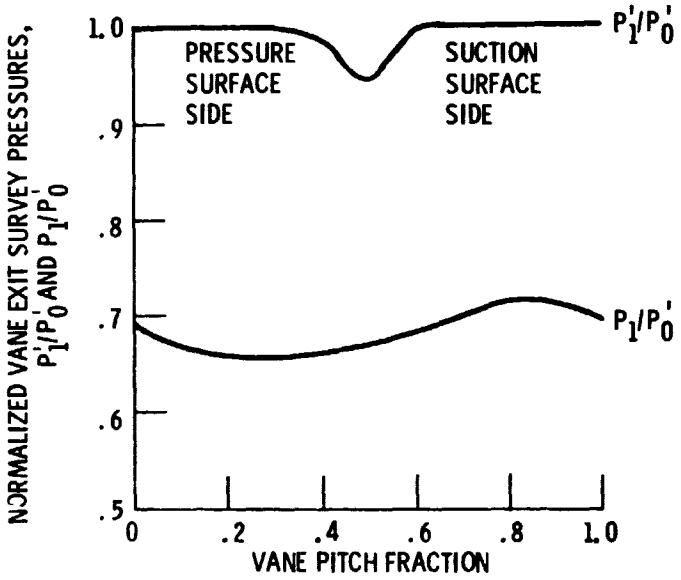

Figure 6. - Typical vane exit survey pressure data.

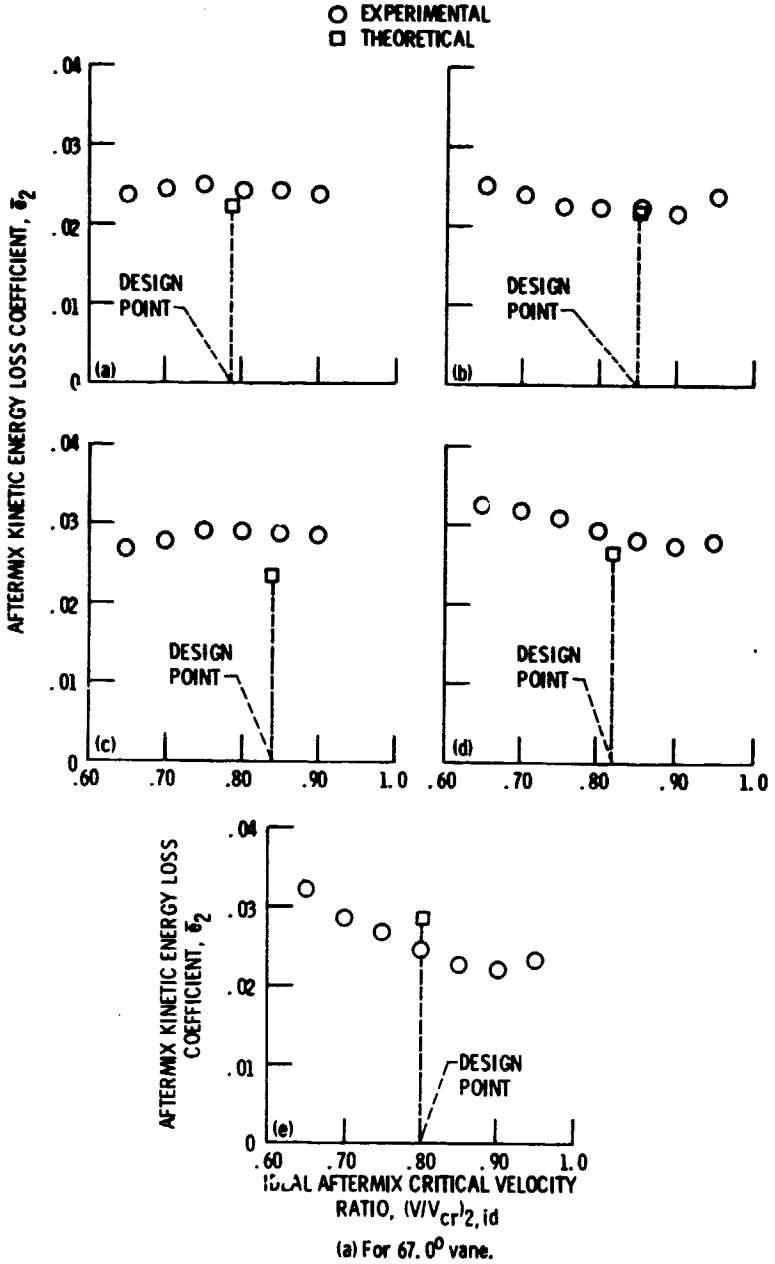

(a) For 67.0° vane.

(b) For 74.9° vane.

(c) For 75.0° vane.

(d) For 77.5° vane.

(e) For 79.6° vane.

Figure 7. - Kinetic energy losses.

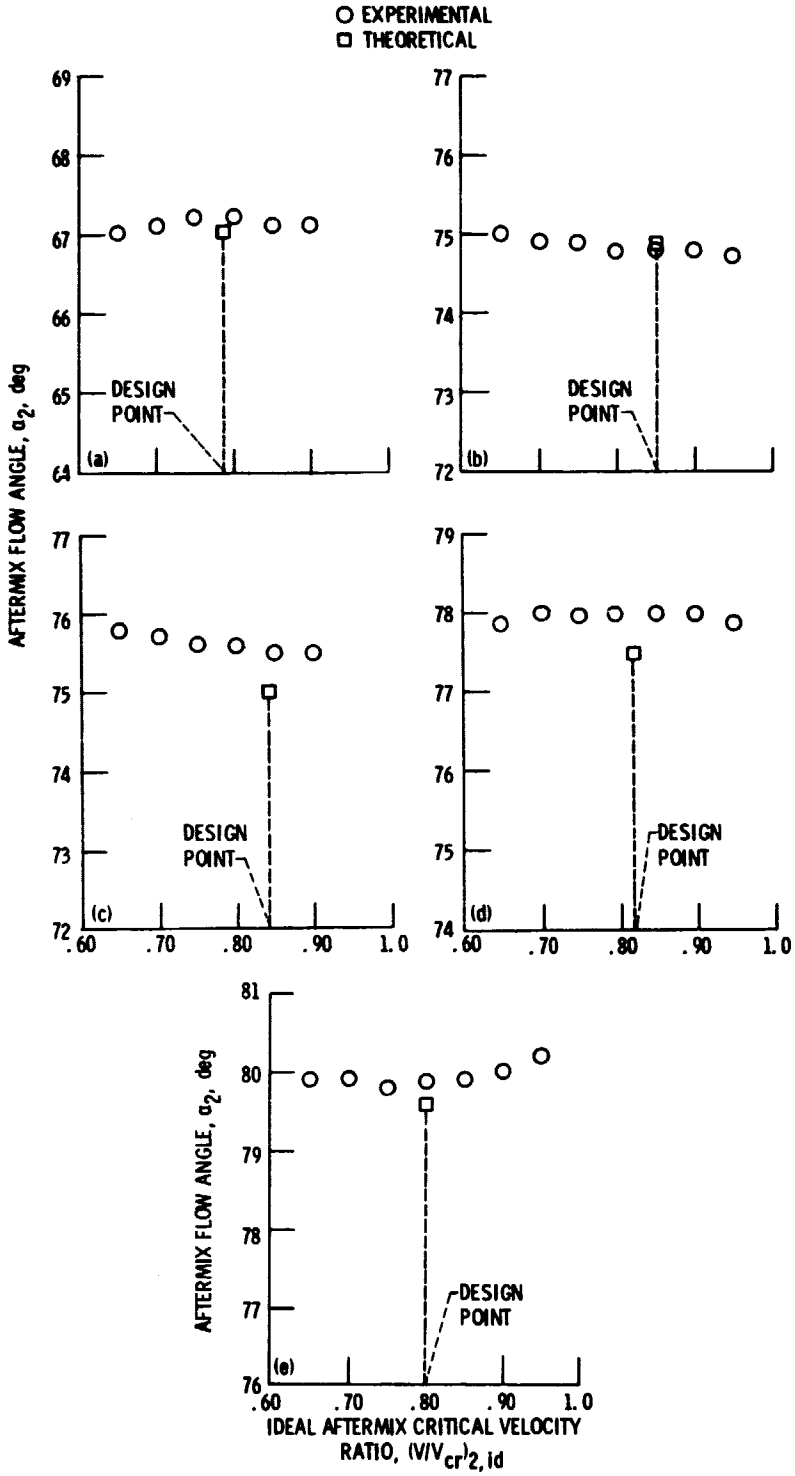

(a) For 67.0° vane.

(b) For 74.9° vane.

(c) For 75.0° vane.

(d) For 77.5° vane.

(e) For 79.6° vane.

Figure 8. - Aftermix flow angles.

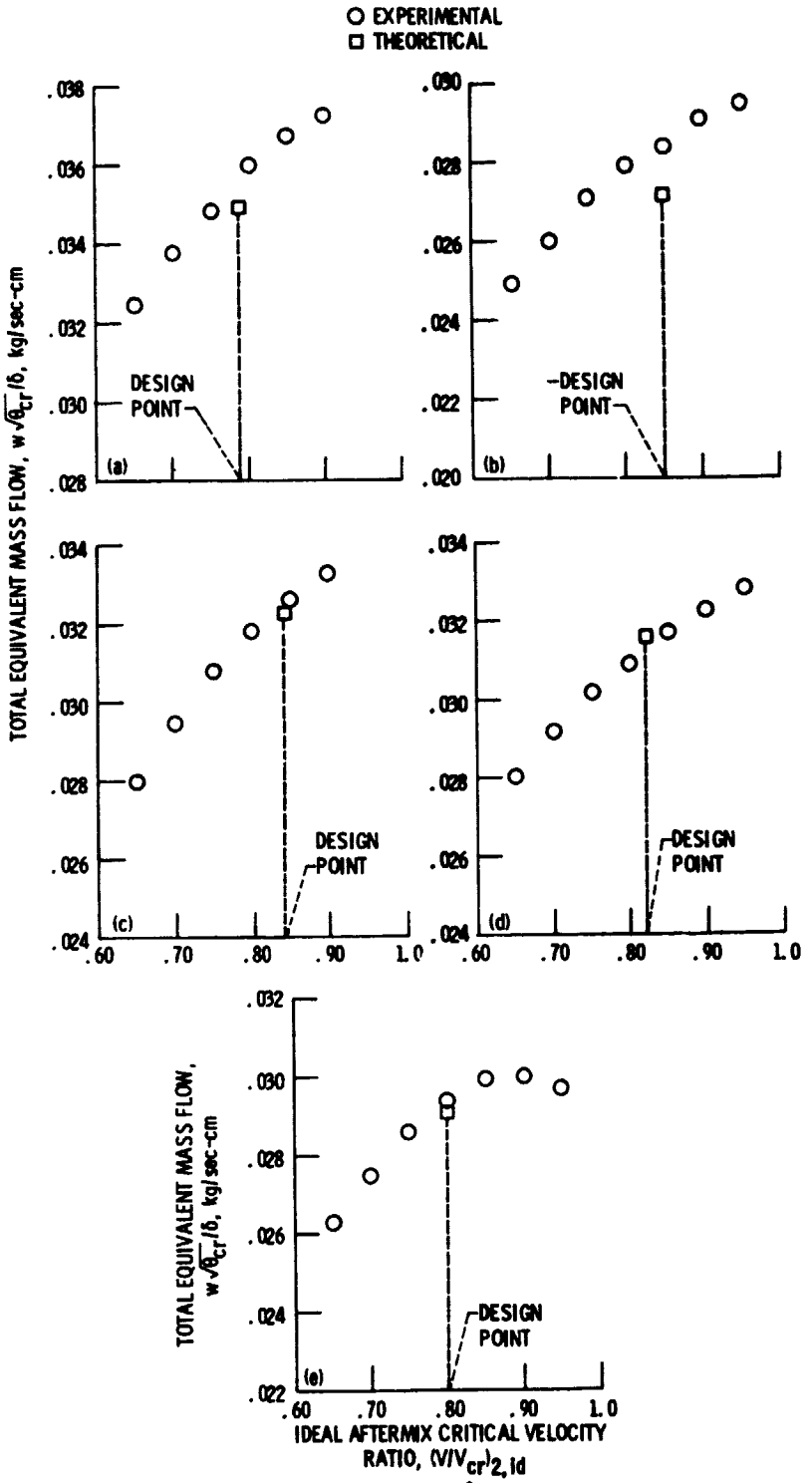

(a) For 67.0° vane.

(b) For 74.9° vane.

(c) For 75.0° vane.

(d) For 77.5° vane.

(e) For 79.6° vane.

Figure 9. - Total equivalent mass flows.

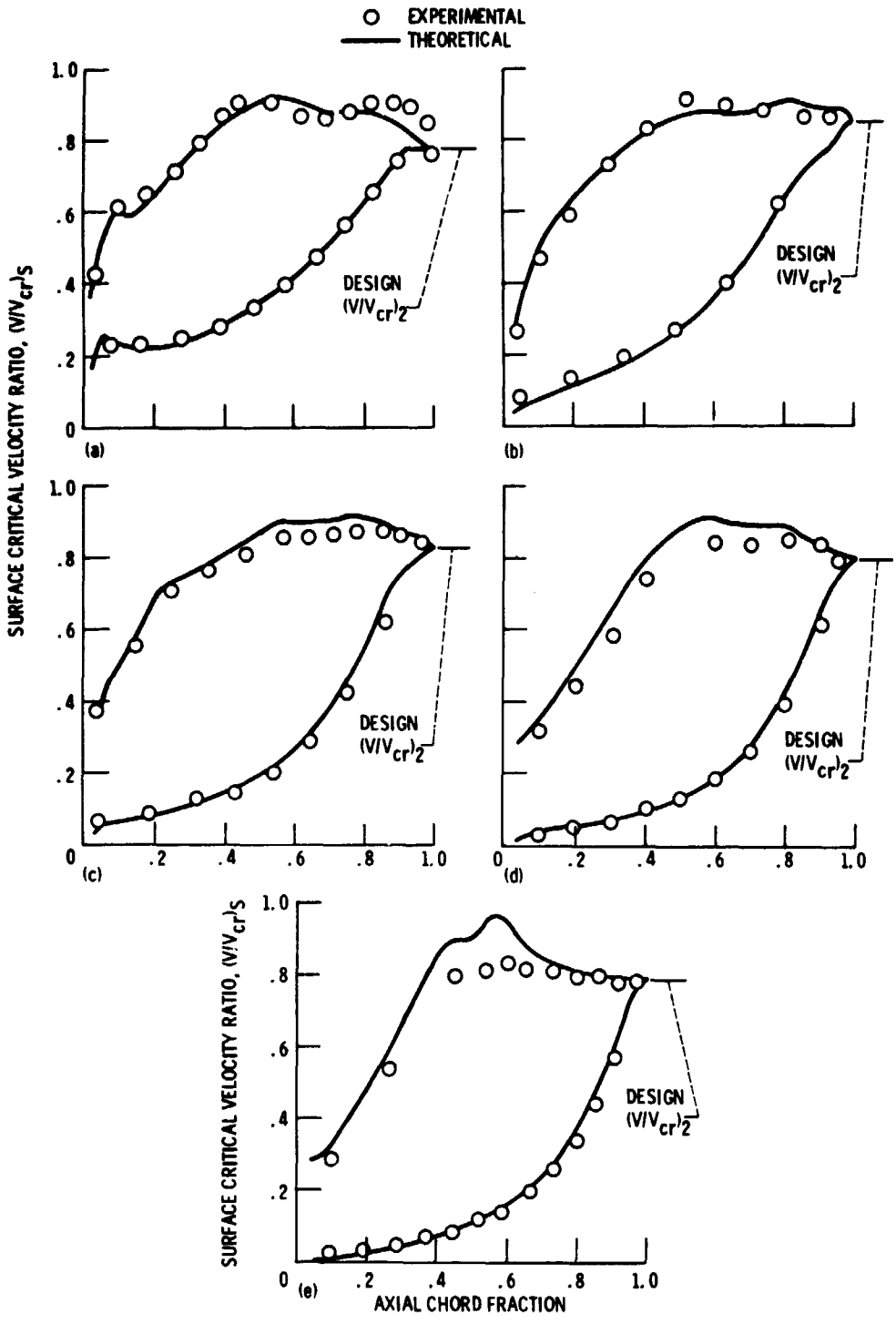

(a) For 67.0° vane.

(b) For 74.9° vane.

(c) For 75.0° vane.

(d) For 77.5° vane.

(e) For 79.6° vane.

Figure 10. - Surface velocity distribution.

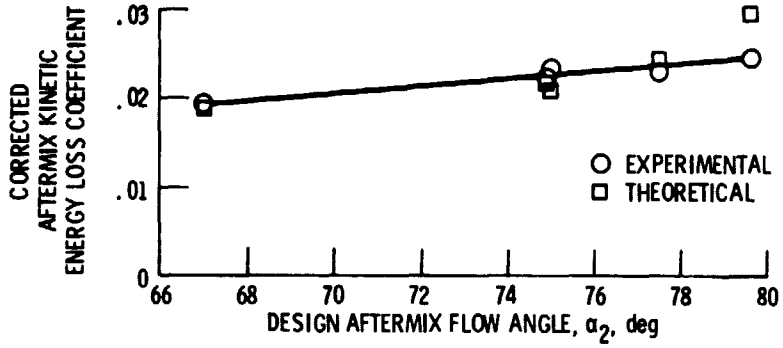

Figure 11. - Comparison of experimental losses corrected to 0.100 cm trailing edge thickness with theoretical losses calculated using 0.100 cm trailing edge thickness.

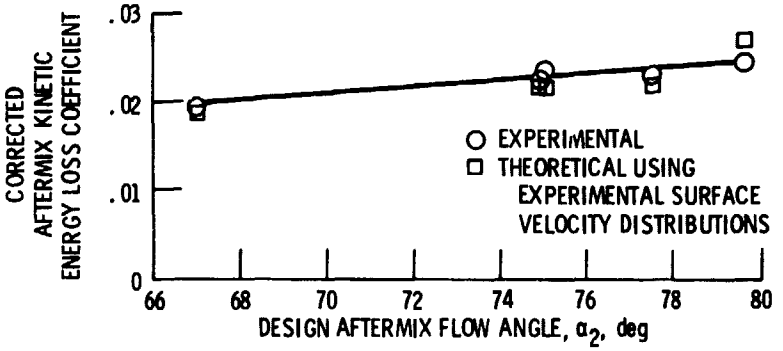

Figure 12. - Comparison of experimental losses corrected to 0.100 cm trailing edge thickness with theoretical losses calculated using 0.100 cm trailing edge thickness and experimental surface velocity distributions.

1. Report No.	2. Government Accession No.	3. Recipient's Catalog No.
NASA TM-82894		

4. Title and Subtitle	5. Report Date
AERODYNAMIC PERFORMANCE OF HIGH TURNING CORE TURBINE VANES IN A TWO-DIMENSIONAL CASCADE	6. Performing Organization Code 505-32-2B

7. Author(s)	8. Performing Organization Report No.
John R. Schwab	E-1272

9. Performing Organization Name and Address	10. Work Unit No.
National Aeronautics and Space Administration Lewis Research Center Cleveland, Ohio 44135	11. Contract or Grant No.

12. Sponsoring Agency Name and Address	13. Type of Report and Period Covered
National Aeronautics and Space Administration Washington, D.C. 20546	Technical Memorandum
	14. Sponsoring Agency Code

15. Supplementary Notes

Prepared for the Eighteenth Joint Propulsion Conference cosponsored by the AIAA, SAE, and ASME, Cleveland, Ohio, June 21-23, 1982.

16. Abstract

Experimental and theoretical aerodynamic performance data are presented for four uncooled high turning core turbine vanes with exit angles of 74.9, 75.0, 77.5, and 79.6 degrees in a two-dimensional cascade. Data for a more conservative 67.0 degree vane are included for comparison. Correction of the experimental aftermix kinetic energy losses to a common 0.100 centimeter trailing edge thickness yields a linear trend of increased loss from 0.020 to 0.025 as the vane exit angle increases from 67.0 to 79.6 degrees. The theoretical losses show a similar trend. The experimental and theoretical vane surface velocity distributions generally agree within approximately five percent, although the suction surface theoretical velocities are generally higher than the experimental velocities as the vane exit angle increases.

17. Key Words (Suggested by Author(s))	18. Distribution Statement
Turbines Aerodynamics	Unclassified - unlimited STAR Category 02

19. Security Classif. (of this report)	20. Security Classif. (of this page)	21. No. of Pages	22. Price*
Unclassified	Unclassified		

* For sale by the National Technical Information Service, Springfield, Virginia 22161